Tabu Search Optimization of Magnetic Sensor Systems for Magnetocardiography

Stephan Lau[1], Roland Eichardt[2], Luca Di Rienzo[3], and Jens Haueisen[2]

[1]Biomagnetic Center, Friedrich-Schiller-University Jena, Jena 07747, Germany
[2]Institute of Biomedical Engineering, Technical University Ilmenau, Ilmenau 98693, Germany
[3]Department of Electrical Engineering, Politecnico di Milano, Milano 20133, Italy

This paper addresses the question of optimal sensor placement for magnetocardiographic field imaging. New magnetic sensor technologies allow less restrictive sensor positioning in this application. We develop a constraint framework for sensor positioning and use tabu search (TS) and particle swarm optimization (PSO) for finding an optimal set of sensors, whereby a new PSO algorithm is designed to fit the needs of our constraint framework. Numerical simulations are carried out with a three compartment boundary element torso model and a multi-dipole heart model. We find an optimal value of about 20 to 30 vectorial sensors and both TS and PSO yield similar sensor distributions. The comparison to sensors on regular grids shows that optimization of vectorial magnetic sensor setups may significantly improve reconstruction quality and that the number of sensors can be reduced.

***Index Terms*—Boundary element methods, inverse problems, magnetostatics, multisensor systems, optimization methods.**

I. Introduction

MAGNETOCARDIOGRAPHIC field imaging (MFI) is a technique used to record contact free the magnetic field distribution and estimate the underlying source distribution in the heart [1]. Typically, the cardiomagnetic fields are recorded with superconducting quantum interference devices (SQUIDs) [2]. SQUIDs are restricted in their positioning to cryostats, since they require liquid helium (low temperature superconductors) or nitrogen (high temperature superconductors) cooling. Recently, however, new technologies of magnetic sensor systems for magnetocardiography (MCG) (e.g., optically pumped magnetic sensors [3]) make less restrictive sensor positioning feasible. Therefore, the general question arises how to optimally place the sensors obeying a technical minimum distance between them. To this end, a typical goal function used in sensor array optimization is the condition number (CN) of the kernel (leadfield) matrix [4].

Since the generation of the kernel matrix for a given position of magnetic sensors is computationally expensive, a pre-computation for a dense enough grid of sensor positions and orientations is needed. Consequently, the search space of the optimization scheme is discretized.

Tabu Search (TS) [5] is a discrete optimization technique that creates in each step new candidate solutions (sets of sensors) in the neighborhood of the current solution that are not classified as tabu (previously examined). Neighbor solutions are created from the current solution by exchanging elements (sensors) with unused elements with the advantage that local minima in the goal function can be overcome.

In order to validate TS optimization results, a new quasi-continuous particle swarm optimizer (PSO) [6] with minimum sensor distance constraint is proposed in the present paper.

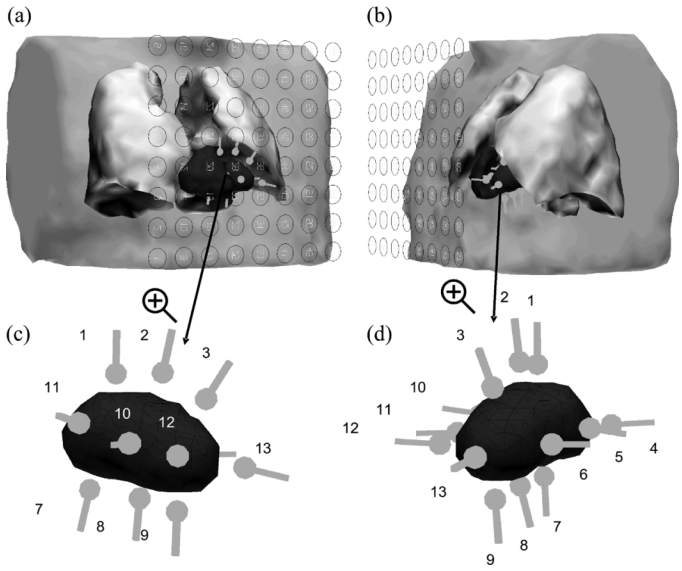

Fig. 1. Sensor plane in front of the boundary element model of torso, lungs, and ventricular blood mass. The source model consists of 13 dipoles.

Swarm intelligence makes use of the gradient. Not one candidate solution is optimized but a swarm of solutions (the particles) is optimized. PSO, like TS, is robust against local minima. At the same time it is a continuous technique, moving the sensors through the search volume smoothly.

II. Computational Methods

A. Simulation Setup

We construct a boundary element method (BEM) (Fig. 1) model out of a three-dimensional magnetic resonance image of a healthy volunteer as described in [7] and [8]. The torso and both lungs are differentiated as three homogeneous compartments, because they have the strongest impact on the forward solution. Average isotropic conductivities of 0.2 S/m (torso) and 0.04 S/m (lungs) are assigned, which are derived from physiological tissue conductivities [9]. Although the myocardial fibers

Digital Object Identifier 10.1109/TMAG.2007.915911

Color versions of one or more of the figures in this paper are available online at http://ieeexplore.ieee.org.

are known to be anisotropic, isotropic conductivities are assumed here since it is difficult to obtain reliable anisotropy information. Additionally, its impact on the external magnetic field was found to be less important than other modeling errors [10]. The ventricular depolarization phase of a heart beat is modeled with the help of 13 electric current dipoles, which are placed regularly around the left ventricle (inside the cardiac muscle). To facilitate this, the ventricular blood volume is segmented (Fig. 1). Magnetic field distributions are computed by means of the freely available SimBio toolbox [11].

By fixing the dipole locations, the inverse problem is linearized and a kernel matrix is set up. The kernel matrix contains information on the geometry of the source space, on the forward BEM model and on the geometry of the sensor array. Each row $L_s(i)$ of the kernel matrix L_s contains the linear coefficients that are required to map a set of dipole amplitudes $\mathbf{p}$ to a signal amplitude $\mathbf{b}(i)$ at a sensor with index i, corresponding to $\mathbf{b} = L_s \cdot \mathbf{p}$ with $\mathbf{b} \in \Re^{s\times 1}$ and $\mathbf{p} \in \Re^{1\times t}$.

To find an optimal setup with r out of altogether s sensors, we first create the kernel matrix $L_s \in \Re^{s\times 1}$ for all s sensors and t sources. The kernel matrix of a subset of r sensors $L_s \in \Re^{r\times t}$ can then be obtained by taking the respective rows of L_S.

The objective of the optimization is to find the kernel matrix $L_r^* \in \Re^{r\times t}$ by choosing the rows of L_S with minimal CN. The kernel matrix with smallest CN has the highest information content. Thus, also the array of the respective sensors is the optimal selection.

B. Tabu Search (TS)

The optimization for the selection of r rows from L_s (and r of s sensors, respectively) is performed by tabu search (TS) [7] with an infinite memory (tabu list).

The sensor search space is discretized in positions by a regular 11×11 grid (distance 2 cm) in front of the torso (similar to [7]). The full directional space is discretized regularly (distance 45°). Our minimum distance of 2 cm is implicitly satisfied by the grid.

To find an optimal configuration with r (between 13 and 100) out of s sensors, we first create the kernel matrix $L_s \in \mathrm{R}^{s\times t}$ for $s = 7502$ sensors (11×11 positions, each with 26 discrete directions) and $t = 13$ sources. The TS optimization is constrained not to select two sensors with same positions.

In our TS algorithm, neighbor solutions L_r are created from the current solution $L_r^{\#}$ by exchanging e rows of $L_r^{\#}$ with unused rows of L_S, which means to use e different sensors in the setup. To make a transition from global to local search, we reduce the number e of exchanged sensors linearly from $s/2$ to 1 over the first 2/3 of the iterations. To prevent reevaluations of any L_r, the tabu list contains information on all previously created matrices (indices of used sensors). The applied TS approach works as follows:

1) create neighbors L_r from the current solution $L_r^{\#}$;
2) compute CN for all L_r that are not in the tabu list;
3) insert newly evaluated L_r into the tabu list;
4) update current solution $L_r^{\#}$, if a new best solution L_r is found in this iteration;
5) continue with 1. or stop, if the maximum number of iterations is reached.

The best out of 10 repetitions is used. The number of iterations and neighbors is chosen to require 10^6 CN computations over all.

C. Particle Swarm Optimization (PSO)

In this study the standard PSO algorithm 2006 [12] ($w = 1/3$, $c = 2$) is implemented and adapted in the object-oriented (C++) framework SimBio [11]. A swarm of particles is randomly initialized with positions and orientations for a fixed number of sensors. The number of particles is $\#_{\text{particles}} = 2\sqrt{5s}$ with 5 being the number of position and orientation parameters (X, Y, Z, Φ, Θ) and s being the number of used sensors. The number of informants per particle is set to exactly 95% of all particles (almost fully informed swarm).

In each iteration, the velocity vector $\mathbf{v}$, describing the individual direction in which the global optimum is expected, is updated using the current vector to the individual best solution $\mathbf{f}$ so far and the informants' best solution $\mathbf{g}$ so far:

$$\mathbf{v}' = w\mathbf{v} + R(c)\cdot(\mathbf{f}-\mathbf{x}) + R(c)\cdot(\mathbf{g}-\mathbf{x}) \tag{1}$$

where the function R returns a random number in $[0, c]$. Second, particles are moved by their velocity vector from the current position $\mathbf{x}$

$$\mathbf{x}' = \mathbf{x} + \mathbf{v}'. \tag{2}$$

Initially, in order to match the available resources of TS, the optimization is repeated up to 1 million goal function evaluations. Since the first runs show a convergence well below 1500 iterations ($1500 \cdot \#_{\text{particles}}$ goal function evaluations) for all simulations this limit is used. To eliminate initialization effects repeated runs are performed up to 1 million goal function evaluations.

PSO is run in a quasi-continuous fashion. The search space is discretized because the repeated computation of kernel matrices is too time consuming. An 85×85 grid (distance 2.5 mm) in the same plane and location is used. Directions are discretized regularly using 30°.

D. Constraint Framework for Continuous PSO

The PSO algorithm is equipped with a constraint restoration strategy. After each PSO iteration, the sensor positions are snapped back into the grid, so that a goal function evaluation is possible. Additionally, the minimum distance is restored by iteratively resolving clashes between sensors with the following algorithm (Fig. 2):

1) pick a sensor with maximum number of clashes;
2) move all clashing sensors away radially;
3) snap into grid without re-violating restored distances;
4) if mean(minimum distance violation) $>$ tolerance, continue with 1, otherwise stop.

For this algorithm, maximum number of 50 iterations is defined. However, this number of iterations is only reached if the number of sensors approaches the maximum number of sensors that the search space can hold. The sensor with maximum number of clashes is the representative (at position $\vec{u}$ in the search volume) of the sensor cloud (Fig. 2) and is not moved, because its position can be expected to be valuable. Each clashing

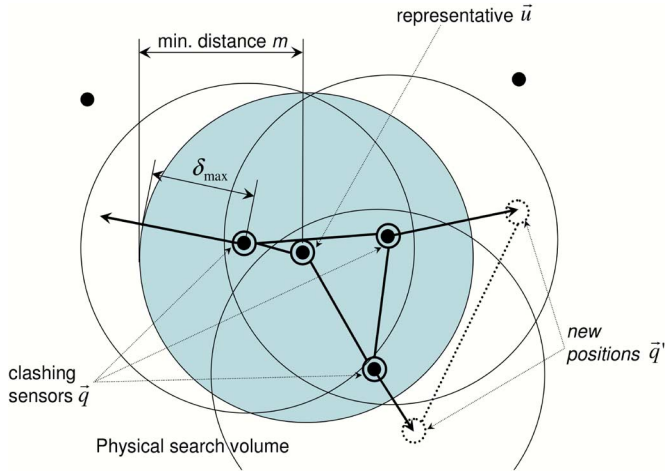

Fig. 2. Restoring the minimum distance in the constraint of PSO. Black dots indicate sensor positions in the search volume and black dots with small circles clashing sensors. Large circles indicate the minimum distance of each sensor, the gray shaded large circle for the representative of the cloud. Exemplary two new sensor positions are indicated by small dotted circles (right).

sensor (at position $\vec{q}$ in the search volume) is moved radially by a length l:

$$\vec{q}' = \vec{q} + l \cdot \frac{\vec{q} - \vec{u}}{|\vec{q} - \vec{u}|} \tag{3}$$

where l is actually a weighted sum according to

$$l = \xi \cdot \delta_{\max} + (1 - \xi) \cdot (m - |\vec{q} - \vec{u}|). \tag{4}$$

The minimum sensor distance m is in this paper 2 cm. The maximum violation $\delta_{\max}$ is defined as the maximum depth of intrusion of any clashing sensor into the space of the representative sensor. The parameter $\xi \in [0,1]$ regulates the influence of $\delta_{\max}$. If $\xi = 0$ the clashing sensors are moved to the edge of the space of the representative sensor, which will result in too close positions of the moved sensors in case they have close to parallel movement vectors. If $\xi = 1$ this is prevented but sensor are moved over relatively large distances and the optimization results are potentially disturbed. We heuristically set ξ to 0.05. The advantage of moving the clashing sensors radially away from the representative sensor is that the clashing sensors themselves are moved as little as possible from the cloud center. At the same time, the distance between two clashing sensors is increased.

The radial movement of sensors could potentially result in a new cloud of clashing sensors. A subsequent radial shift would possibly move the clashing sensors back to the first cloud. This would result in oscillations when applied in an iterative procedure as outlined above. This problem may theoretically yield infinite oscillations in the collinear case. Thus, we implemented a small additional random angle to the radial shift (here set to 7°).

The *snap into the grid without re-violating restored distances* (Step 3 in algorithm above) is realized by selecting the closest grid node to the desired new position, which is at the same time outside the volume occupied by the representative sensor.

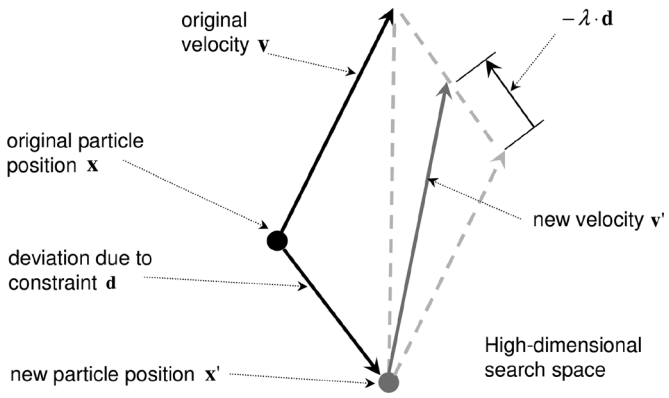

Fig. 3. Correction of the velocity of particles in the PSO algorithm. The black dot indicates the old particle position and the gray dot indicates the new, shifted particle position. The new velocity (gray) is adjusted with the help of λ. Note that particles encode multiple sensor positions and directions and are thus defined in high-dimensional search space.

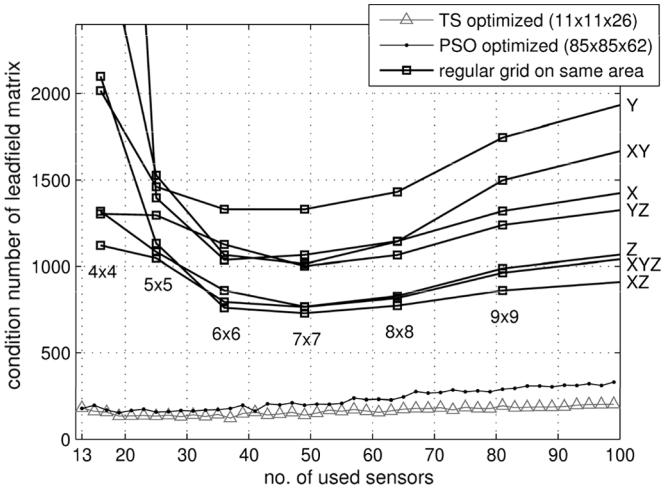

Fig. 4. CNs of optimized and regular grid setups (X = all sensors aligned with positive X-axis, etc.) for a range of numbers of sensors.

E. Modifications to PSO Due to Constraints

From the perspective of the optimizer the fulfillment of the constraints in each iteration results in a deviation $\mathbf{d}$ from $\mathbf{x}$ ($\mathbf{x}' = \mathbf{x} + \mathbf{d}$) in high-dimensional space. The current velocity vector $\mathbf{v}$ should then be adjusted (Fig. 3). The new velocity $\mathbf{v}'$ is set using the scaled deviation vector:

$$\mathbf{v}' = \mathbf{v} - \lambda \cdot \mathbf{d} \tag{5}$$

where $\lambda \in [0,1]$. The parameter λ is set heuristically to 0.5. Keeping the old velocity ($\lambda = 0$) would distract the optimization process, while the case $\lambda = 1$ would overcompensate the shift.

III. Numerical Results

Both optimization techniques reduce the CN significantly when compared to a regular grid with the same number of aligned sensors (Fig. 4). In these noise-free simulations, the optimal number of sensors s is around 20–30 for both TS and PSO. The optimal number of sensors for the regular grids is between 36 (6×6) and 49 (7×7). The strongest gain (largest difference between regular grids and optimized sensor setups)

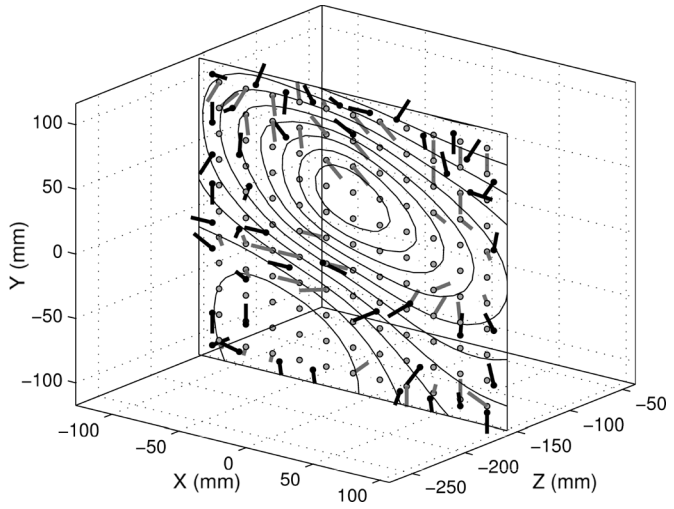

Fig. 5. TS (gray/green bars) and PSO (black/blue bars) optimized setups of 45 sensors on top of 11 × 11 grid (circles) and a magnetic field map of the X component (thin solid lines). The sensor grid is positioned centrally in front of the torso.

is achieved for setups with low number of sensors. This is expected because the lower the number of sensors available the higher the information gain of optimal sensor positions.

TS and PSO produce very similar CNs for about $s < 45$ (Fig. 4). For denser sensor setups ($s > 45$), TS performs a bit better. The higher CNs for PSO at higher numbers of sensors can be explained by the difficulties PSO encounters in moving sensors in a densely populated search volume. Moreover, slight differences between the two optimization approaches can be explained by the fact that the direction discretization *was* different for PSO (30°) and TS (45°).

On regular grids, the CNs for the sensor directions show significant differences. As expected for single component sensors the Z-direction sensors exhibit best CNs, while X and Y perform worse. When Z-direction sensors are combined with X or X and Y sensors, yet lower CNs are obtained, which is in line with our previous findings [7].

TS and PSO optimized setups show similar positions and orientations of sensors (Fig. 5). The main difference to regular grids is that sensors tend to be placed in areas of strong magnetic field gradient. Many of the optimal sensor positions are close to the boundary of the search volume (see edges of the square in Fig. 5). This indicates that the search volume might not have been large enough.

Similar results of PSO and TS and repeated runs (results not shown) indicate the existence of few strong minima in the goal function. Thus, there is a potential to develop application specific setups.

IV. Conclusion

Both TS and PSO optimization of vector sensor setups may improve reconstruction robustness and reduce the number of sensors while retaining information in terms of CN.

A strength of TS is its ability to handle dense sensor setups, because sensors are not gradually moved but exchanged. A limitation of TS is that it can only handle a combinatorial optimization on a pre-selected set of sensor positions. The new quasi-continuous PSO optimization incorporates the gradient and spatial closeness information into the optimization while being robust against local minima of the goal function.

For future work, projection method based [13], [14] and lower error bound based [15] sensor setup optimizations and more extensive search volumes are planned.

Acknowledgment

This work was supported in part by the state of Thuringia/ Germany (2006FE0096) under participation of the European Union within the European Funds for Regional Development (EFRE).

References

[1] U. Leder, J. Haueisen, M. Huck, and H. Nowak, "Non-invasive imaging of arrhythmogenic left-ventricular myocardium after infarction," *LANCET*, vol. 352, p. 1825, Dec. 1998.

[2] W. Andrä and H. Nowak, *Magnetism in Medicine*. Weinheim, Germany: Wiley-VCH, 2006.

[3] G. Bison, R. Wynands, and A. Weis, "Optimization and performance of an optical cardiomagnetometer," *J. Opt. Soc. Amer. B*, vol. 22, pp. 77–87, Jan. 2005.

[4] L. Rouve, L. Schmerber, O. Chadebec, and A. Foggia, "Optimal magnetic sensor location for spherical harmonics identification applied to radiated electrical devices," *IEEE Trans. Magn.*, vol. 42, no. 4, pp. 1167–1170, Apr. 2006.

[5] F. Glover and M. Laguna, *Tabu Search*. Oxford, U.K.: Kluwer Academic, 2001.

[6] A. P. Engelbrecht, *Fundamentals of Computational Swarm Intelligence*. Chichester, U.K.: Wiley, 2005.

[7] C. M. Arturi, L. Di Rienzo, and J. Haueisen, "Information content in single-component versus three-component cardiomagnetic fields," *IEEE Trans. Magn.*, vol. 40, no. 3, pp. 631–634, Mar. 2004.

[8] L. Di Rienzo, J. Haueisen, and C. M. Arturi, "Three component magnetic field data: impact on minimum norm solutions in a biomedical application," *COMPEL*, vol. 24, pp. 869–881, Jul. 2005.

[9] L. A. Geddes and L. E. Baker, "The specific resistance of biological material," *Med. & Biol. Eng.*, vol. 5, pp. 271–293, May 1967.

[10] C. Ramon *et al.*, "Effects of myocardial anisotropy on the torso current flow patterns, potentials and magnetic fields," *Phys. Med. Biol.*, vol. 45, pp. 1141–1150, May 2000.

[11] J. Fingberg *et al.*, "Bio-numerical simulations with SimBio," *NEC Res. Dev.*, vol. 44, pp. 140–145, Jan. 2003.

[12] M. Clerc, Standard PSO 2006. May 2007 [Online]. Available: http://www.particleswarm.info

[13] M. Nalbach and O. Dössel, "Comparison of sensor arrangements of MCG and ECG with respect to information content," *Physica C*, vol. 372, pp. 254–258, Aug. 2002.

[14] L. Di Rienzo and J. Haueisen, "Numerical comparison of sensor arrays for magnetostatic linear inverse problems based on a projection method," *COMPEL*, vol. 26, pp. 356–367, Apr. 2007.

[15] L. Di Rienzo and J. Haueisen, "Theoretical lower error bound for comparative evaluation of sensor arrays in magnetostatic linear inverse problems," *IEEE Trans. Magn.*, vol. 42, no. 11, pp. 3669–3673, Nov. 2006.

Manuscript received June 24, 2007. Corresponding author: L. Di Rienzo (e-mail: luca.dirienzo@polimi.it).